

# Automated Calculation Scheme for $\alpha^n$ Contributions of QED to Lepton $g-2$ : New Treatment of Infrared Divergence for Diagrams without Lepton Loops

T. Aoyama,<sup>1</sup> M. Hayakawa,<sup>2</sup> T. Kinoshita,<sup>3</sup> and M. Nio<sup>4</sup>

<sup>1</sup>*Institute of Particle and Nuclear Studies,*

*High Energy Accelerator Research Organization (KEK), Tsukuba, 305-0801, Japan*

<sup>2</sup>*Department of Physics, Nagoya University, Nagoya, 464-8602, Japan*

<sup>3</sup>*Laboratory for Elementary-Particle Physics,*

*Cornell University, Ithaca, New York 14853, U.S.A.*

<sup>4</sup>*Theoretical Physics Laboratory, RIKEN, Wako, 351-0198, Japan*

## Abstract

We have developed an efficient algorithm for the subtraction of infrared divergences that arise in the evaluation of QED corrections to the anomalous magnetic moment of lepton ( $g-2$ ). By incorporating this new algorithm, we have extended the automated code-generating system developed previously to deal with diagrams without internal lepton loops (called *q-type*), which produced convergent integrals when applied to diagrams that have only ultraviolet-divergent subdiagrams of vertex type. The new system produces finite integrals for all *q-type* diagrams, including those that contain self-energy subdiagrams and thus exhibit infrared-divergent behavior. We have thus far verified the system for the sixth- and eighth-order cases. We are now evaluating 6354 vertex diagrams of *q-type* that contribute to the tenth-order lepton  $g-2$ .

PACS numbers: 13.40.Em, 14.60.Cd, 14.70.Bh, 11.15.Bt, 12.20.Ds

## I. INTRODUCTION

The magnetic moment anomaly of electron, also called the electron  $g-2$ , has been measured with steadily increased precision since its discovery in 1947 [1]. The latest experiment using Penning trap with cylindrical cavity updates the best previous value [2] of the electron  $g-2$  to [3]

$$a_e = 1\,159\,652\,180.85\,(76) \times 10^{-12} \quad [0.76\text{ppb}]. \quad (1)$$

Here,  $a_e = \frac{1}{2}(g-2)$  and the numeral in the parenthesis represents uncertainty in the last two digits of the value. The uncertainty has been reduced by a factor 5.5 over the previous best value.

Theoretically, the electron  $g-2$  is almost entirely accounted for by the QED corrections, and thus it has provided the most stringent test of the validity of QED. The dominant contribution comes from the interaction between photons and electrons alone (referred to as mass-independent term), and it is given as a function of the fine structure constant  $\alpha$ . An important by-product of the study of the electron  $g-2$  is that a very precise value of  $\alpha$  can be obtained from the measurement and the theory of  $a_e$ , assuming the validity of QED. The value of  $\alpha$  thus determined is [4]

$$\alpha^{-1}(a_e) = 137.035\,999\,070\,(12)(37)(90) \quad [0.71\text{ppb}], \quad (2)$$

where uncertainties are due to the  $\alpha^4$  term, an educated guess of the  $\alpha^5$  term [5], and the experiment (1). The value (2) is by far the most precise determination of  $\alpha$  at present<sup>1</sup>.

As is seen from Eq. (2) the measurement uncertainty in  $\alpha(a_e)$  is only a factor 2.5 larger than that of the theory which is mostly due to the unknown  $\alpha^5$  term. When the experimental data improves further, the  $\alpha^5$  term will become the largest source of unresolved systematic errors. This is why an explicit evaluation of  $\alpha^5$  term is urgently needed.

The mass-independent contribution to the  $\alpha^5$  term involves 12672 Feynman diagrams, which can be divided into 32 gauge-invariant sets. We classify them into 6 super sets (Set I–VI) according to their structures (see Figs. I–VI of Ref. [8]). The largest and the most difficult is the Set V, which consists of 6354 diagrams that have no lepton loops (we call them *q-type*) and form a single gauge-invariant set. The difficulty of the Set V stems from

---

<sup>1</sup> Note that the value given in Eq. (2) includes small changes in the tenth-order estimate [5] and in the hadronic light-by-light contribution [5, 6], and thus deviates from  $\alpha^{-1}$  given in Ref. [7].

the fact that many of them, besides being gigantic, have very large number of ultraviolet (UV) and infrared (IR) divergences.

In the previous approach employed in the calculation of sixth-order and eighth-order diagrams the subtraction terms of UV divergence were constructed by a procedure called *K*-operation [9], which is based on a simple power counting at a UV-divergent singularity. In order to deal with UV divergences, let us regularize each relevant photon propagator by introducing the Feynman cut-off

$$\frac{1}{k^2} \longrightarrow \frac{1}{k^2 - \lambda^2} - \frac{1}{k^2 - \Lambda^2} = - \int_{\lambda^2}^{\Lambda^2} \frac{dL}{(k^2 - L)^2}, \quad (3)$$

where  $\Lambda$  and  $\lambda$  are UV-cutoff and IR-cutoff, respectively. Suppose the diagram  $\mathcal{G}$  has a UV-divergent *vertex* subdiagram  $\mathcal{S}$ . Let  $M_{\mathcal{G}}$  be the magnetic moment contribution of  $\mathcal{G}$ . Then the operation of  $\mathbb{K}_{\mathcal{S}}$  on  $M_{\mathcal{G}}$  creates an integral  $\mathbb{K}_{\mathcal{S}}M_{\mathcal{G}}$  which has the same UV cutoff  $\Lambda$  as  $M_{\mathcal{G}}$  itself and yet factorizable into the product shown on the right-hand side:

$$\mathbb{K}_{\mathcal{S}}M_{\mathcal{G}} = L_{\mathcal{S}}^{\text{UV}} M_{\mathcal{G}/\mathcal{S}}, \quad (4)$$

where  $L_{\mathcal{S}}^{\text{UV}}$  is the leading UV-divergent part (referred to as the most-contracted term) of the vertex renormalization constant  $L_{\mathcal{S}}$ , and  $M_{\mathcal{G}/\mathcal{S}}$  is the magnetic moment projection for the reduced diagram that is obtained from  $\mathcal{G}$  by shrinking  $\mathcal{S}$  to a point. It is important to note that the factorization in Eq.(4) does not work unless both sides are well-defined integrals (made finite by the Feynman cut-off or some other regularization). Throughout this paper let us assume that all UV-divergent integrals are regularized by the Feynman cutoff. Of course the Feynman cutoff is not needed for convergent integrals, and the limit  $\Lambda \rightarrow \infty$  must be taken after the renormalization is carried out.

In Ref. [10] it was shown that this scheme of UV-subtraction can be incorporated into an automating algorithm without change. In the case of Set V diagrams of tenth-order we were able to obtain FORTRAN codes for 2232 vertex diagrams containing only vertex subdiagrams (represented by 135 Ward-Takahashi-summed diagrams [see Eq. (6)]) out of the total of 6354 vertex diagrams (represented by 389 Ward-Takahashi-summed diagrams). A preliminary numerical evaluation of these integrals by VEGAS [11] shows that UV divergences are removed completely.

In case where  $\mathcal{S}$  is a *self-energy* subdiagram inserted between consecutive lines  $i$  and  $j$  of

$\mathcal{G}$ , the action of  $\mathbb{K}_{\mathcal{S}}$  on  $M_{\mathcal{G}}$  yields a somewhat more complicated factorization

$$\mathbb{K}_{\mathcal{S}}M_{\mathcal{G}} = \delta m_{\mathcal{S}}^{\text{UV}} M_{\mathcal{G}/\mathcal{S}(i^*)} + B_{\mathcal{S}}^{\text{UV}} M_{\mathcal{G}/[\mathcal{S},j]}, \quad (5)$$

where  $\delta m_{\mathcal{S}}^{\text{UV}}$  and  $B_{\mathcal{S}}^{\text{UV}}$  are the leading UV divergent parts of the mass renormalization constant  $\delta m_{\mathcal{S}}$  and the wave-function renormalization constant  $B_{\mathcal{S}}$ , respectively. The  $*$  in  $M_{\mathcal{G}/\mathcal{S}(i^*)}$  indicates that it has a two-point vertex between the lines  $i$  and  $j$ .  $\mathcal{G}/[\mathcal{S},j]$  denotes a diagram obtained by shrinking both  $\mathcal{S}$  and line  $j$  to points.

This method works as far as subtraction of UV divergence is concerned. However, it complicates the handling of IR divergence because of the fact that the unrenormalized  $M_{\mathcal{G}}$  as well as its self-mass counter term  $\delta m_{\mathcal{S}}M_{\mathcal{G}/\mathcal{S}(i^*)}$  have a linear or worse IR divergence. In the calculation of the eighth-order case we encountered such linear IR divergences in two diagrams<sup>2</sup>  $M_{16}$  and  $M_{18}$  as well as in some renormalization constants [9, 12]. This problem has been handled by subtracting the linear IR divergence by an *ad hoc* subtraction term.

However, such an *ad hoc* approach will become very complicated in the tenth-order case. Furthermore, it will present a severe obstacle to automation. Thus, we have developed an alternative approach to subtraction of the linear (and worse) IR divergence which is entirely systematic and fits well in the scheme of automated code generation. It generates FORTRAN codes of the renormalized and finite amplitudes for all diagrams of the Set V very rapidly, which are ready for numerical integration.

The aim of this paper is to present the new approach for constructing the IR subtraction term in an automated manner. We also report its implementation.

The organization of the paper is as follows. In Sec. II we briefly summarize our formulation of the numerical evaluation of lepton  $g-2$  and the scheme of subtractive UV renormalization. In Sec. III we present a new scheme for identifying IR divergences that may appear in a complex manner. The construction of subtraction integrals for those divergences is described in Sec. IV. In Sec. V we show the concrete procedure of code generation and its implementation. Sec. VI is devoted to conclusion and discussion. An example of the identification of IR subtraction terms is given in Appendix A.

---

<sup>2</sup>  $M_{16}$  and  $M_{18}$  share the structure which is obtained by inserting two self-energy subdiagrams, one is of the second order and the other is of the fourth order, into the second-order magnetic moment term.

## II. UNRENORMALIZED AMPLITUDE AND UV DIVERGENCES

In this section we briefly summarize our formulation for evaluating QED contribution to the anomalous magnetic moment of leptons by numerical means [9, 13, 14]. It involves the construction of amplitudes for Feynman diagrams and the renormalization of ultraviolet divergences. We note that the substructure called *forests* plays a crucial role in organizing the UV renormalization and also accounts for our subtraction scheme of infrared divergences discussed in the later sections.

### A. Anomalous Magnetic Moment of Lepton

The anomalous magnetic moment  $a_e$  is given by the static limit of the magnetic form factor that is related to the proper vertex part  $\Gamma^\nu$ . We evaluate the QED contribution to  $a_e$  in the framework of perturbation theory by the series expansion with respect to  $\alpha/\pi$ , where  $\alpha$  is the fine structure constant.

In our formulation we employ a relation derived from the Ward-Takahashi identity

$$\Lambda^\nu(p, q) \simeq -q^\mu \left[ \frac{\partial \Lambda_\mu(p, q)}{\partial q_\nu} \right]_{q \rightarrow 0} - \frac{\partial \Sigma(p)}{\partial p_\nu} \quad (6)$$

between the self-energy part  $\Sigma(p)$  and the sum of vertex parts  $\Lambda^\nu(p, q)$  obtained by inserting an external vertex in the lepton lines of  $\Sigma$  in all possible ways. Here, the momentum of the incoming lepton  $p - \frac{1}{2}q$  and that of the outgoing lepton  $p + \frac{1}{2}q$  are on the mass shell so that  $p$  and  $q$  satisfy  $p^2 = m^2 - \frac{1}{4}q^2$  and  $p \cdot q = 0$ . Eq. (6) enables us to turn the evaluation of a set of vertex diagrams into the evaluation of a single self-energy-like diagram. This approach reduces the number of independent diagrams substantially.

The magnetic moment anomaly of a  $2n$ th-order diagram  $\mathcal{G}$  is given by an integral over loop momenta of a product of vertices and propagators of lepton and photon. It is turned into a parametric integral over Feynman parameters  $z_i$  by the Feynman integration formula. Carrying out the momentum integration analytically, we can express the resulting amplitude in a concise form:

$$M_{\mathcal{G}}^{(2n)} = \left(-\frac{1}{4}\right)^n (n-1)! \int (dz)_{\mathcal{G}} \left[ \frac{1}{n-1} \left( \frac{E_0 + C_0}{U^2 V^{n-1}} + \frac{E_1 + C_1}{U^3 V^{n-2}} + \cdots \right) + \left( \frac{N_0 + Z_0}{U^2 V^n} + \frac{N_1 + Z_1}{U^3 V^{n-1}} + \cdots \right) \right], \quad (7)$$

where  $(dz)_G = \prod dz_i \delta(1 - \sum_i z_i)$ . The factor  $(\alpha/\pi)^n$  is omitted for simplicity. It is implicitly assumed that the Feynman cutoff (3) is introduced whenever it is necessary.

The quantities  $C_k$ ,  $E_k$ ,  $N_k$ , and  $Z_k$  are polynomials of symbols called building blocks  $B_{ij}$ ,  $A_i$ , and  $C_{ij}$  [13]. The symbols  $B_{ij}$  and  $U$  are homogeneous polynomials of Feynman parameters, related to the flow of loop momenta on the diagram. The symbol  $A_i$  is called scalar current that is associated with the flow of the external momentum  $p$ . It is constructed from  $B_{ij}$ ,  $U$ , and  $\{z_i\}$ . The symbol  $C_{ij}$  is also constructed from  $B_{ij}$ ,  $U$ , and  $\{z_i\}$ . The symbol  $V$  in the denominator is a function defined by

$$V = \sum_i z_i - G, \quad G = \sum_i z_i A_i, \quad (8)$$

where the summation is over the lepton lines only and the rest mass of the lepton is set to  $m = 1$  for simplicity.

## B. Subtraction of UV Divergences

The amplitude constructed above is UV-divergent except for the case  $n = 1$ . To achieve pointwise cancellation of these divergences we adopt here the subtractive renormalization.

The UV divergence arises when some of the loop momenta go to infinity. In the Feynman parametric space it corresponds to a particular regime in which the sum of relevant Feynman parameters tends to zero. We prepare the subtraction term in the form of an integral such that it cancels the singularity of the original integrand at a singular point of the integration domain. These subtraction integrals are constructed from the original integrand by the  $K$ -operation. As was noted already they factorize exactly into a product (or a sum of products) of lower-order magnetic projection and a UV-divergent part of the renormalization constant. (See Eq. (4) and Eq. (5).)

In the prescription described above, we only subtracted away a part of renormalization constants. This is because the integral becomes highly intractable if those renormalization constants are treated as a whole. To carry out the standard on-shell renormalization, we have to take account of the difference, *e.g.*  $L_S - L_S^{\text{UV}}$  in Eq. (4). Similarly for the self-mass term and the wave-function renormalization term. We adopt two-step renormalization, and adjust the differences afterward by collecting all contributions over the diagrams. We call it the residual renormalization step.

### C. Forests

A diagram may have complicated divergence structure due to nested singularities. The whole structure of UV divergences is managed by Zimmermann's forest formula. A forest is a set of divergent subdiagrams and each forest corresponds to a particular emergence of divergence.

First we introduce an inclusion relation of subdiagrams as follows. If two subdiagrams share neither vertex nor line, they are called *disjoint*. If a subdiagram  $\mathcal{S}$  is included in the other subdiagram  $\mathcal{S}'$  in the sense that all vertices and lines of  $\mathcal{S}$  are also the elements of  $\mathcal{S}'$ ,  $\mathcal{S}$  is *included* in  $\mathcal{S}'$ . When  $\mathcal{S}$  and  $\mathcal{S}'$  have common vertices and/or lines but one is not included in the other, they are *overlapping*. In this case there are some vertices and lines of  $\mathcal{S}$  that are not the elements of  $\mathcal{S}'$ .

A forest  $f$  is defined as a set of subdiagrams of which any two elements are not overlapping. It is called normal forest when the diagram  $\mathcal{G}$  itself is not an element of the forest. The whole set of (normal) forests is found by generating all possible combinations of subdiagrams and disregarding any combinations in which a pair of elements are overlapping.

Noting that the  $K$ -operation can be defined for each  $\mathcal{S}$ , we can define the UV-finite amplitude  $\underline{M}_{\mathcal{G}}$  by the formula

$$\underline{M}_{\mathcal{G}} = M_{\mathcal{G}} + \sum_{f \in \mathfrak{F}} \prod_{\mathcal{S} \in f} (-\mathbb{K}_{\mathcal{S}}) M_{\mathcal{G}}, \quad (9)$$

where the summation is taken over the set  $\mathfrak{F}$  of the normal forests of the diagram  $\mathcal{G}$ , and the product means the successive application of  $K$ -operations.

### III. IR DIVERGENCES

The magnetic form factor is free from UV- and IR-divergences once it is fully renormalized. However, individual diagrams suffer from IR divergences which cancel out only after all diagrams are combined.

The root cause of IR divergence is the vanishing of the denominator of the photon propagator  $1/k^2$  in the limit  $k \rightarrow 0$ . This is, however, not the sufficient condition since it gives a finite result on integration over the 4-dimensional momentum  $k$ . In order that it becomes divergent, it must be enhanced by vanishing of the denominators of at least two lepton

propagators due to some kinematical constraints. Typically, this happens when the momentum of each of these lepton propagators is constrained by sharing a three-point vertex with the soft photon and an external on-shell lepton line. When the external momentum  $p$  is constrained by the on-shell condition  $p^2 = m^2$ , the lepton propagator in question behaves as

$$\frac{1}{(p+k)^2 - m^2} = \frac{1}{2p \cdot k + k^2} \sim \frac{1}{2p \cdot k} \quad (10)$$

for  $k \rightarrow 0$ . These lepton propagators will be called “enhancers”. The logarithmic IR divergence takes place when the  $k$ -integration is carried out and the soft photon singularity is assisted by two enhancers. When the vertex Feynman diagram  $\mathcal{G}(k)$  in question has a self-energy subdiagram, we find three enhancers due to the kinematical constraint of the two-point vertex so that we find the IR divergence to be linear. The IR divergence becomes even severer when the diagram  $\mathcal{G}(k)$  has more than one self-energy subdiagram which effectively bring in a number of two-point vertices.

To handle the IR divergences, we adopt again a subtractive approach in which an integral of IR subtraction terms is constructed in such a way that it cancels out the IR-divergence of the integral  $M_{\mathcal{G}}^{(2n)}$  of Eq. (7) point-by-point in the Feynman parameter space.

First we briefly summarize a scheme called *I*-operation [9] which has been developed and employed for the calculation of sixth- and eighth-order calculations.

In the Feynman-parametric representation, the IR divergence is caused by vanishing of the denominator function  $V$  of Eq.(8) in the corner of the integration domain characterized by

$$\begin{aligned} z_i &= \mathcal{O}(\delta) && \text{if } i \text{ is an lepton line in } \mathcal{R}, \\ z_i &= \mathcal{O}(1) && \text{if } i \text{ is a photon line in } \mathcal{R}, \\ z_i &= \mathcal{O}(\epsilon), \quad \epsilon \sim \delta^2 && \text{if } i \in \mathcal{S}, \end{aligned} \quad (11)$$

where  $\mathcal{R} = \mathcal{G}/\mathcal{S}$ . In this limit the denominator  $V$  vanishes as  $\mathcal{O}(\delta^2)$ . (The last condition is actually an artifact of the condition  $\sum_i z_i = 1$ , which can be readily lifted.)

If two lepton propagators participate in the enhancement, we obtain a *logarithmic* IR divergence. In this case we can construct an IR subtraction term by a simple power counting rule and an *I*-operation similar to the *K*-operation of the UV divergent case. For the subdiagram  $\mathcal{R} = \mathcal{G}/\mathcal{S}$  the *I*-operation  $I_{\mathcal{R}}$  is defined as follows:

- (a) In the limit (11) keep only terms with lowest power of  $\epsilon$  and  $\delta$  in  $U, B_{ij}, A_i$ .



(b) Make the following replacements:

$$U \rightarrow U_{\mathcal{S}} U_{\mathcal{R}}, \quad V \rightarrow V_{\mathcal{S}} + V_{\mathcal{R}}, \quad F \rightarrow F_0[L_{\mathcal{R}}] F_{\mathcal{S}}, \quad (12)$$

where  $F_0[L_{\mathcal{R}}]$  is the non-contracting term of the vertex renormalization constant defined on  $\mathcal{R}$ , and  $F_{\mathcal{S}}$  is the product of  $\gamma$  matrices and  $D_i^\mu$  operators for the diagram  $\mathcal{S}$ . (See Ref. [9] for definitions.)

This procedure creates an integral defined on the parametric space of  $M_{\mathcal{G}}$ . By construction it factorizes as

$$L_{\mathcal{R}(k)}[F_0] M_{\mathcal{S}} + M_{\mathcal{R}^*}[I] \Delta \delta \tilde{m}_{\mathcal{S}}. \quad (13)$$

For precise definitions of quantities quoted above see Ref. [9].

In the following, we see that for the lepton  $g-2$  of the  $q$ -type diagrams, there are two kinds of sources of enhancement. These two types of divergences may occur simultaneously in a complicated manner. We will introduce a new scheme modeled on the previous approach for identifying the emergence of the divergences. In this scheme the identification relies on examining the shape of the diagram that allows diagrammatic treatment systematically without the need for close examination of the integrand, and it is also suited for automated treatment.

### A. IR Divergence Caused by Residual Self-mass

One type of IR divergence appears as a consequence of our particular treatment of the UV divergences by means of  $K$ -operation. Suppose a diagram  $\mathcal{G}$  has a self-energy subdiagram  $\mathcal{S}$ . As is readily seen from the analysis of Feynman diagrams, this divergence is not the source of real problem since it must be canceled exactly by the mass-renormalization counterterm  $\delta m_{\mathcal{S}} M_{\mathcal{G}/\mathcal{S}(i^*)}$ , where  $\delta m_{\mathcal{S}}$  is the (UV-divergent) self-mass associated with the subdiagram  $\mathcal{S}$  defined on the mass shell. The reduced magnetic moment amplitude  $M_{\mathcal{G}/\mathcal{S}(i^*)}$  is the one that has a linear IR divergence. As a consequence

$$M_{\mathcal{G}} - \delta m_{\mathcal{S}} M_{\mathcal{G}/\mathcal{S}(i^*)} \quad (14)$$

is free from linear IR divergence. Although this cancellation is analytically valid, however, it is not a pointwise cancellation in the domain of  $M_{\mathcal{G}}$ . Our problem is thus to translate the

second term into a form which is defined in the same domain as that of  $M_{\mathcal{G}}$  and cancels the IR divergence of  $M_{\mathcal{G}}$  point-by-point.

Now, as was noted in Eq. (5) the  $K$ -operation for the subdiagram  $\mathcal{S}$  acting on  $M_{\mathcal{G}}$  creates

$$\mathbb{K}_{\mathcal{S}}M_{\mathcal{G}} = \delta m_{\mathcal{S}}^{\text{UV}} M_{\mathcal{G}/\mathcal{S}(i^*)} + B_{\mathcal{S}}^{\text{UV}} M_{\mathcal{G}/[\mathcal{S},j]}. \quad (15)$$

If we find an integral what causes pointwise cancellation of the linear IR divergence in the domain of  $M_{\mathcal{G}}$  and also produces the factorization as

$$\widetilde{\delta m}_{\mathcal{S}} M_{\mathcal{G}/\mathcal{S}(i^*)} \quad (16)$$

where

$$\widetilde{\delta m}_{\mathcal{S}} \equiv \delta m_{\mathcal{S}} - \delta m_{\mathcal{S}}^{\text{UV}}, \quad (17)$$

then from Eqs. (15) and (16) we would have

$$\mathbb{K}_{\mathcal{S}}M_{\mathcal{G}} + \widetilde{\delta m}_{\mathcal{S}} M_{\mathcal{G}/\mathcal{S}(i^*)} = \delta m_{\mathcal{S}} M_{\mathcal{G}/\mathcal{S}(i^*)} + B_{\mathcal{S}}^{\text{UV}} M_{\mathcal{G}/[\mathcal{S},j]}. \quad (18)$$

If we schematically introduce an operator  $\mathbb{R}_{\mathcal{S}}$  that produces the integral of Eq. (16) as

$$\mathbb{R}_{\mathcal{S}}M_{\mathcal{G}} \equiv \widetilde{\delta m}_{\mathcal{S}} M_{\mathcal{G}/\mathcal{S}(i^*)}, \quad (19)$$

Eq. (18) would then be written as

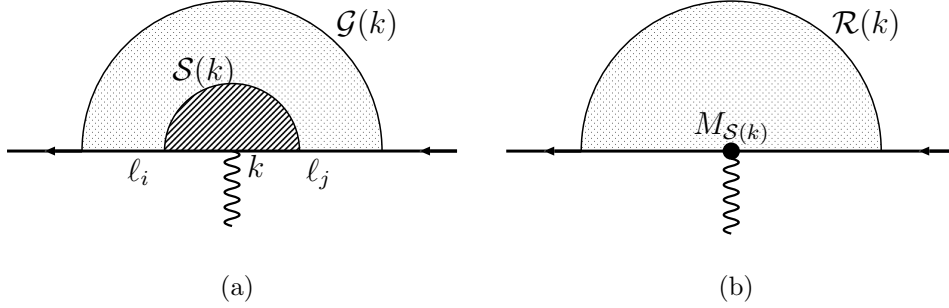
$$(\mathbb{K}_{\mathcal{S}} + \mathbb{R}_{\mathcal{S}})M_{\mathcal{G}} = \delta m_{\mathcal{S}} M_{\mathcal{G}/\mathcal{S}(i^*)} + B_{\mathcal{S}}^{\text{UV}} M_{\mathcal{G}/[\mathcal{S},j]}. \quad (20)$$

It turns out that it is not difficult to construct such an integral. Furthermore, it can be readily incorporated in our automation algorithm. We call this subtraction scheme as the residual self-mass subtraction, or “ $R$ -subtraction” operation.

## B. Modified $I$ -subtraction operation

After the linear IR divergences are disposed by the  $K$ -operation and  $R$ -subtraction operation we are still left with logarithmic IR divergences. To treat these divergences let us consider a vertex diagram  $\mathcal{G}(k)$  which has a subdiagram  $\mathcal{S}(k)$ . Here  $k$  refers to an external photon vertex attached to a lepton line  $\ell_k$  of  $\mathcal{S}$ . The reduced diagram  $\mathcal{R} \equiv \mathcal{G}(k)/\mathcal{S}(k)$  is connected to  $\mathcal{S}(k)$  by lepton lines  $\ell_i$  and  $\ell_j$ . (See Fig. 1(a).)

FIG. 1: A vertex diagram  $\mathcal{G}(k)$  and a subdiagram  $\mathcal{S}(k)$ , The reduced vertex diagram  $\mathcal{R}(k)$  with a vertex  $M_{\mathcal{S}(k)}$ .



This diagram exhibits an IR-divergent behavior when the momenta of (all or some) photons in  $\mathcal{R}$  go to zero, accompanied by the enhancers  $\ell_i$  and  $\ell_j$ . The substructure  $\mathcal{S}(k)$  to which these enhancers are attached can be considered as a magnetic moment of the lower order. Thus the amplitude in this limit becomes that of the diagram  $\mathcal{R}(k)$  obtained by replacing  $\mathcal{S}(k)$  by a vertex that is weighted by  $M_{\mathcal{S}(k)}$ , as shown in Fig. 1(b).  $\mathcal{R}(k)$  develops a logarithmic IR divergence as is easily verified by power counting.

Since we are dealing with the Ward-Takahashi-summed diagram defined by Eq. (6), we have to consider the sum of contributions of vertex diagrams  $\mathcal{S}(k)$  which are obtained by inserting an external vertex  $k$  to the self-energy-like diagram  $\mathcal{S}$  in every possible way. In the calculation of the diagram  $\mathcal{G}$ , the IR singularity associated with the substructure  $\mathcal{S}$  has a form that consists of contributions from the vertex diagram  $\mathcal{R}(k)$  and the magnetic projection of the diagram  $\mathcal{S}$ . The IR singularity is contained in the vertex renormalization constant  $L_{\mathcal{R}(k)}$ .

For the explicit expression of the IR subtraction term that cancels the singularity in the above, we consider the term

$$\tilde{L}_{\mathcal{G}/\mathcal{S}(k)} M_{\mathcal{S}}, \quad (21)$$

where  $\tilde{L}$  is the residual part of the vertex renormalization constant

$$\tilde{L}_{\mathcal{G}/\mathcal{S}(k)} \equiv L_{\mathcal{G}/\mathcal{S}(k)} - L_{\mathcal{G}/\mathcal{S}(k)}^{\text{UV}}. \quad (22)$$

We construct an integral that corresponds to Eq. (21) in the domain of  $M_{\mathcal{G}}$ . We call this subtraction scheme as the “ $I$ -subtraction” operation.

Note that the subtraction scheme for IR divergence adopted here is different from that of Ref.[9]. We now choose as the IR subtraction term the part of  $L_{\mathcal{G}/\mathcal{S}(k)}$  which excludes the overall UV divergent part but includes a finite part  $\Delta L_{\mathcal{G}/\mathcal{S}(k)}$  left out in the previous method. This simplifies the handling of the IR problem considerably.

The magnetic moment part  $M_{\mathcal{S}}$  may have UV and IR divergences, which also have to be subtracted. The UV subdivergences of  $M_{\mathcal{S}}$  will be treated in a similar manner to the UV subdivergences of  $L$ . The IR divergence that is related to the nested singularity is discussed in the next subsection.

### C. Nested Singularity

We have introduced the operations for identifying the subtraction terms called *I*- and *R*-subtraction operations corresponding to two types of divergences. There may appear more than one source of IR divergences that lead to complicated divergence structure. They are treated by combinations of *I*-/*R*-subtraction operations conducted by *annotated forests* described later.

By generalizing Eq. (19) the *R*-subtraction operation  $\mathbb{R}_{\mathcal{S}}$  for a self-energy subdiagram  $\mathcal{S}$  is defined by

$$\mathbb{R}_{\mathcal{S}}\underline{M}_{\mathcal{G}} \equiv \delta m_{\mathcal{S}}^{\text{R}} \underline{M}_{\mathcal{G}/\mathcal{S}(i^*)}, \quad (23)$$

where the operator  $\mathbb{R}_{\mathcal{S}}$  acts on the UV-finite amplitude  $\underline{M}_{\mathcal{G}}$  of the self-energy-like diagram  $\mathcal{G}$  and generates a product of a residual part of mass renormalization constant  $\delta m_{\mathcal{S}}^{\text{R}}$  defined by Eq. (24) and a UV-finite lower-order amplitude  $\underline{M}_{\mathcal{G}/\mathcal{S}(i^*)}$ . The reduced diagram  $\mathcal{G}/\mathcal{S}(i^*)$  is obtained from  $\mathcal{G}$  by shrinking  $\mathcal{S}$  to a point. The term  $\delta m_{\mathcal{S}}^{\text{R}}$  is defined as a residual part of the mass renormalization constant  $\delta m_{\mathcal{S}}$  defined on the mass shell by subtracting the leading UV divergence (referred to as the most-contracted term)  $\delta m_{\mathcal{S}}^{\text{UV}}$  and the subdivergences as

$$\delta m_{\mathcal{S}}^{\text{R}} \equiv \delta m_{\mathcal{S}} - \delta m_{\mathcal{S}}^{\text{UV}} + \sum_f \prod_{\mathcal{S}' \in f} (-\mathbb{K}_{\mathcal{S}'} ) \widetilde{\delta m}_{\mathcal{S}}. \quad (24)$$

$\widetilde{\delta m}_{\mathcal{S}} \equiv \delta m_{\mathcal{S}} - \delta m_{\mathcal{S}}^{\text{UV}}$  may also have extra UV divergences due to its substructures that are subtracted by the *K*-operations as above. Here, the summation is taken over the normal forests of the subdiagram  $\mathcal{S}$ .

The *I*-subtraction operation  $\mathbb{I}_{\mathcal{S}}$  for a self-energy subdiagram  $\mathcal{S}$  is defined by

$$\mathbb{I}_{\mathcal{S}}\underline{M}_{\mathcal{G}} \equiv L_{\mathcal{G}/\mathcal{S}(k)}^{\text{R}} \underline{M}_{\mathcal{S}}, \quad (25)$$

where the operator  $\mathbb{I}_{\mathcal{S}}$  acts on the UV-finite amplitude  $\underline{M}_{\mathcal{G}}$  of the self-energy-like diagram  $\mathcal{G}$  and generates a product of a residual part of vertex renormalization constant  $L_{\mathcal{G}/\mathcal{S}(k)}^{\text{R}}$  defined by Eq. (26) and a UV-finite lower-order amplitude  $\underline{M}_{\mathcal{S}}$ . Here, the diagram  $\mathcal{R}(k) \equiv \mathcal{G}/\mathcal{S}(k)$  is given from  $\mathcal{G}$  by replacing  $\mathcal{S}$  by an external photon vertex labelled by  $k$ . The term  $L_{\mathcal{R}(k)}^{\text{R}}$  is defined as a residual part of the vertex renormalization constant  $L_{\mathcal{R}(k)}$  defined on the mass shell by subtracting the leading UV divergence (referred to as the most-contracted term)  $L_{\mathcal{R}(k)}^{\text{UV}}$  and the subdivergences as

$$L_{\mathcal{R}(k)}^{\text{R}} \equiv L_{\mathcal{R}(k)} - L_{\mathcal{R}(k)}^{\text{UV}} + \sum_f \prod_{S' \in f} (-\mathbb{K}_{S'}) \tilde{L}_{\mathcal{R}(k)}. \quad (26)$$

$\tilde{L}_{\mathcal{R}(k)} \equiv L_{\mathcal{R}(k)} - L_{\mathcal{R}(k)}^{\text{UV}}$  may also have extra UV divergences due to its substructures that have been subtracted by the  $K$ -operations. The summation in Eq. (26) is taken over the normal forests of the diagram  $\mathcal{R}(k)$ .

For a diagram  $\mathcal{G}$  containing a single self-energy subdiagram  $\mathcal{S}$ , the associated IR divergences are treated by those two types of operations, and the IR-finite amplitude is thus given by

$$\Delta M_{\mathcal{G}} = \underline{M}_{\mathcal{G}} - \mathbb{I}_{\mathcal{S}} \underline{M}_{\mathcal{G}} - \mathbb{R}_{\mathcal{S}} \underline{M}_{\mathcal{G}}. \quad (27)$$

When the diagram has more than one such self-energy subdiagram, the IR divergences due to all those subdiagrams have to be subtracted away. The finite amplitude free from both IR and UV divergences are provided schematically by

$$\Delta M_{\mathcal{G}} = \prod_{\mathcal{S}} (1 - \mathbb{I}_{\mathcal{S}} - \mathbb{R}_{\mathcal{S}}) \underline{M}_{\mathcal{G}}, \quad (28)$$

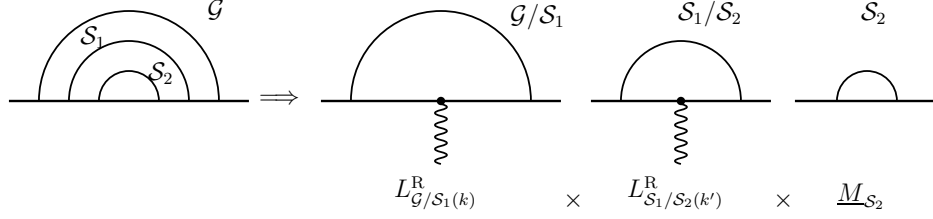
where the product is taken over all self-energy subdiagrams of the diagram  $\mathcal{G}$ .

By expanding the product in Eq. (28), we are lead to a forest-like structure which is analogous to the renormalization of UV divergences. In this case, a forest consists of only self-energy subdiagrams, and each subdiagram is assigned a distinction of  $R$ -subtraction or  $I$ -subtraction. We call such a forest “annotated forest”. Eq. (28) is thus turned into a sum over all annotated forests  $\tilde{f}$  as

$$\sum_{\tilde{f}} (-\mathbb{I}_{\mathcal{S}_i}) \cdots (-\mathbb{R}_{\mathcal{S}_j}) \cdots \underline{M}_{\mathcal{G}}, \quad (29)$$

where  $\mathcal{S}_i, \dots$  and  $\mathcal{S}_j, \dots$  are elements of the annotated forest  $\tilde{f}$  that are assigned to  $I$ -subtraction operations and  $R$ -subtraction operations, respectively. Those operators act on the amplitude  $\underline{M}_{\mathcal{G}}$  successively in an order given below.

FIG. 2: Successive operations of two  $I$ -subtractions for subdiagrams  $\mathcal{S}_1$  and  $\mathcal{S}_2$  that satisfy  $\mathcal{S}_1 \supset \mathcal{S}_2$ . They yield a product of component terms shown on the right-hand side.



By construction of  $I$ - and  $R$ -operators, there are some annotations that are not accepted. To see which annotations are allowed, it is sufficient to examine the cases in which two self-energy subdiagrams are concerned. The inclusion relation of two self-energy subdiagrams is disjoint or inclusive. Therefore, the possible patterns are exhausted by the cases in which both subdiagrams are assigned to  $I$ -operators, both subdiagrams are assigned to  $R$ -operators, or one subdiagram is assigned to  $I$ -operator and the other to  $R$ -operator, for two self-energy subdiagrams which are disjoint or inclusive. We elucidate on those cases separately as follows.

First we consider the case which involves two  $I$ -subtractions. Recall that the action of operator  $\mathbb{I}_{\mathcal{S}_1}$  is given in Eq. (25). It is found that an extra operation of operator  $\mathbb{I}_{\mathcal{S}_2}$  for the subdiagram  $\mathcal{S}_2$  must have its domain in  $M_{\mathcal{S}_1}$ . Therefore the subdiagrams have to respect the relation  $\mathcal{S}_1 \supset \mathcal{S}_2$ . Otherwise, the operation of  $\mathbb{I}_{\mathcal{S}_2}$  turns to zero. It leads to a rule that subdiagrams for  $I$ -operators must satisfy that one subdiagram is included in the other, and a pair of  $I$ -operators for disjoint subdiagrams  $\mathcal{S}_1 \cap \mathcal{S}_2 = \emptyset$  is not allowed in the annotation. The ordering of  $I$ -subtraction operators is given by  $\mathbb{I}_{\mathcal{S}_2}\mathbb{I}_{\mathcal{S}_1}$  for  $\mathcal{S}_1 \supset \mathcal{S}_2$ . (The outer subdiagrams are operated first.)

$$\mathbb{I}_{\mathcal{S}_2}\mathbb{I}_{\mathcal{S}_1}\underline{M}_{\mathcal{G}} = L_{\mathcal{G}/\mathcal{S}_1(k)}^R L_{\mathcal{S}_1/\mathcal{S}_2(k')}^R \underline{M}_{\mathcal{S}_2} \quad \text{for } \mathcal{S}_1 \supset \mathcal{S}_2. \quad (\text{See Fig. 2.}) \quad (30)$$

The  $R$ -operator for a subdiagram  $\mathcal{S}_1$  acts as Eq. (23). If an extra operator of  $\mathbb{R}_{\mathcal{S}_2}$  is applied,  $\mathcal{S}_2$  and the reduced diagram  $\mathcal{G}/\mathcal{S}_1$  ( $i_1^*$ ) must share some parts. Thus  $\mathcal{S}_1$  is included in  $\mathcal{S}_2$ ,  $\mathcal{S}_1 \subset \mathcal{S}_2$ , or  $\mathcal{S}_1$  and  $\mathcal{S}_2$  are disjoint. The ordering of two  $R$ -operators is given by<sup>3</sup>

<sup>3</sup> The operation of  $\mathbb{R}_{\mathcal{S}_2}$  in this case is actually recognized as  $\mathbb{R}_{\mathcal{S}_2/\mathcal{S}_1}$ .

FIG. 3: Successive operations of two  $R$ -subtractions for subdiagrams  $\mathcal{S}_1$  and  $\mathcal{S}_2$  that satisfy  $\mathcal{S}_1 \subset \mathcal{S}_2$ .

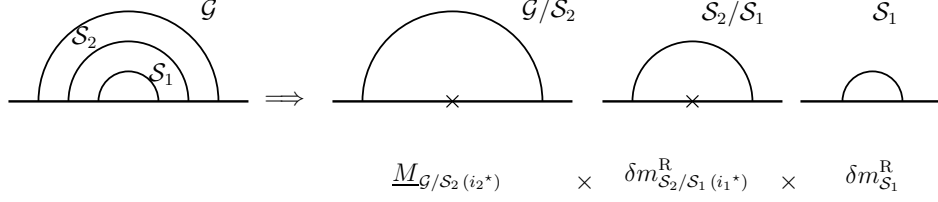
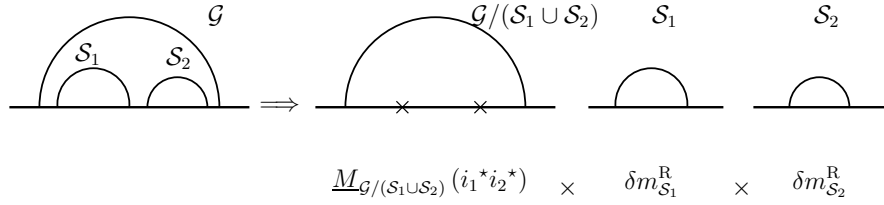


FIG. 4: Successive operations of two  $R$ -subtractions for subdiagrams  $\mathcal{S}_1$  and  $\mathcal{S}_2$  when they are disjoint,  $\mathcal{S}_1 \cap \mathcal{S}_2 = \emptyset$ .



$\mathbb{R}_{\mathcal{S}_2} \mathbb{R}_{\mathcal{S}_1}$  for  $\mathcal{S}_1 \subset \mathcal{S}_2$ . (The inner subdiagrams are operated first.)

$$\mathbb{R}_{\mathcal{S}_2} \mathbb{R}_{\mathcal{S}_1} \underline{M}_{\mathcal{G}} = \underline{M}_{\mathcal{G}/\mathcal{S}_2}(i_2^*) \delta m_{\mathcal{S}_2/\mathcal{S}_1}^{\mathcal{R}}(i_1^*) \delta m_{\mathcal{S}_1}^{\mathcal{R}} \quad \text{for } \mathcal{S}_1 \subset \mathcal{S}_2. \quad (\text{See Fig. 3.}) \quad (31)$$

For disjoint subdiagrams, the ordering is indifferent,

$$\mathbb{R}_{\mathcal{S}_2} \mathbb{R}_{\mathcal{S}_1} \underline{M}_{\mathcal{G}} = \mathbb{R}_{\mathcal{S}_1} \mathbb{R}_{\mathcal{S}_2} \underline{M}_{\mathcal{G}} = \underline{M}_{\mathcal{G}/(\mathcal{S}_1 \cup \mathcal{S}_2)}(i_1^* i_2^*) \delta m_{\mathcal{S}_2}^{\mathcal{R}} \delta m_{\mathcal{S}_1}^{\mathcal{R}} \quad \text{for } \mathcal{S}_1 \cap \mathcal{S}_2 = \emptyset. \quad (\text{See Fig. 4.}) \quad (32)$$

Next we consider the case in which there are two operators  $\mathbb{I}_{\mathcal{S}_1}$  and  $\mathbb{R}_{\mathcal{S}_2}$ . Since  $\mathbb{I}_{\mathcal{S}_1}$  yields  $\underline{M}_{\mathcal{S}_1}$  and  $\mathbb{R}_{\mathcal{S}_2}$  yields  $\underline{M}_{\mathcal{G}/\mathcal{S}_2}(i_2^*)$ ,  $\mathcal{S}_1$  and  $\mathcal{G}/\mathcal{S}_2$  must share some parts, *i.e.*  $\mathcal{S}_1 \supset \mathcal{S}_2$  or  $\mathcal{S}_1 \cap \mathcal{S}_2 = \emptyset$ . For the case  $\mathcal{S}_1 \supset \mathcal{S}_2$ , the successive operations yield

$$\mathbb{R}_{\mathcal{S}_2} \mathbb{I}_{\mathcal{S}_1} \underline{M}_{\mathcal{G}} = \mathbb{R}_{\mathcal{S}_2} (L_{\mathcal{G}/\mathcal{S}_1}^{\mathcal{R}} \underline{M}_{\mathcal{S}_1}) = L_{\mathcal{G}/\mathcal{S}_1}^{\mathcal{R}} \underline{M}_{\mathcal{S}_1/\mathcal{S}_2}(i_2^*) \delta m_{\mathcal{S}_2}^{\mathcal{R}}, \quad (\text{See Fig. 5.}) \quad (33)$$

For the disjoint case  $\mathcal{S}_1 \cap \mathcal{S}_2 = \emptyset$ , it is given as

$$\mathbb{I}_{\mathcal{S}_1} \mathbb{R}_{\mathcal{S}_2} \underline{M}_{\mathcal{G}} = \mathbb{I}_{\mathcal{S}_1} \left( \underline{M}_{\mathcal{G}/\mathcal{S}_2}(i_2^*) \delta m_{\mathcal{S}_2}^{\mathcal{R}} \right) = L_{\mathcal{G}/\mathcal{S}_2/\mathcal{S}_1(k)}^{\mathcal{R}}(i_2^*) \underline{M}_{\mathcal{S}_1} \delta m_{\mathcal{S}_2}^{\mathcal{R}}, \quad (\text{See Fig. 6.}) \quad (34)$$

The case with  $\mathcal{S}_1 \subset \mathcal{S}_2$  is prohibited.

To summarize, an IR-finite amplitude for a self-energy-like diagram  $\mathcal{G}$  is obtained by subtracting away all IR divergences associated with its self-energy subdiagrams. They can

FIG. 5: Successive operations of  $I$ -subtraction for subdiagram  $\mathcal{S}_1$  and  $R$ -subtraction for subdiagram  $\mathcal{S}_2$  when they satisfy  $\mathcal{S}_1 \supset \mathcal{S}_2$ .

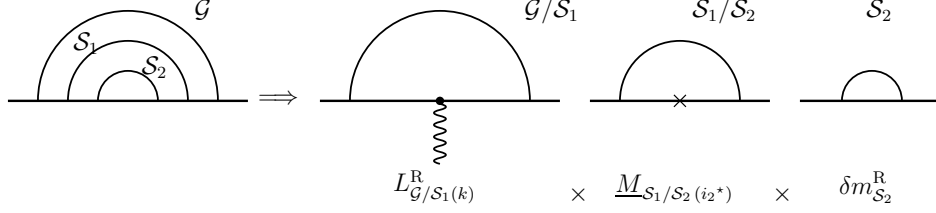
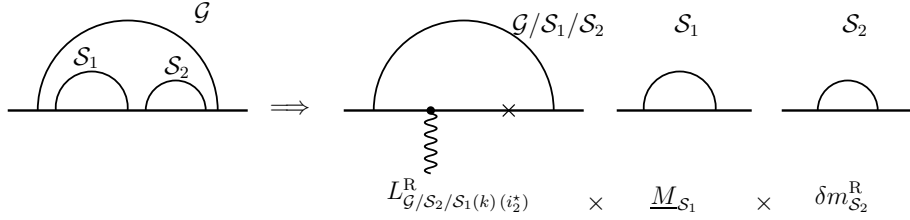


FIG. 6: Successive operations of  $I$ -subtraction for subdiagram  $\mathcal{S}_1$  and  $R$ -subtraction for subdiagram  $\mathcal{S}_2$  when they are disjoint,  $\mathcal{S}_1 \cap \mathcal{S}_2 = \emptyset$ .



be identified by applying two types of subtraction operations to the amplitude, called  $I$ -subtraction operation ( $\mathbb{I}_{\mathcal{S}}$ ) and  $R$ -subtraction operation ( $\mathbb{R}_{\mathcal{S}}$ ), for a set of annotated forests similar to Zimmermann's forests for UV divergences. An annotated forest consists of self-energy subdiagrams, to each of which a distinction of  $I$ -subtraction or  $R$ -subtraction operation is assigned. By construction, the annotation has to respect the assignment rules:

- subdiagrams assigned to  $I$ -subtraction operations are included one another,
- a subdiagram  $\mathcal{S}'$  assigned to  $R$ -subtraction operation does not include a subdiagram  $\mathcal{S}$  assigned to  $I$ -subtraction operation.

The IR-finite amplitude is thus given by

$$\Delta M_{\mathcal{G}} = \underline{M}_{\mathcal{G}} + \sum_{\tilde{f} \in \tilde{\mathcal{F}}} (-\mathbb{I}_{\mathcal{S}_i}) \cdots (-\mathbb{R}_{\mathcal{S}_j}) \cdots \underline{M}_{\mathcal{G}}, \quad (35)$$

in which the summation is taken over all annotated forest  $\tilde{f} = \{\mathcal{S}_i, \dots, \mathcal{S}_j, \dots\}$ . (Recall that  $\underline{M}_{\mathcal{G}}$  is UV-finite.) The allowed combinations of the operators, including their ordering, are listed as follows:



- i)  $\mathbb{I}_{\mathcal{S}_i} \cdot \mathbb{I}_{\mathcal{S}_j}$  for  $\mathcal{S}_i \subset \mathcal{S}_j$ ,
- ii)  $\mathbb{R}_{\mathcal{S}_i} \cdot \mathbb{R}_{\mathcal{S}_j}$  for  $\mathcal{S}_i \supset \mathcal{S}_j$ ,
- iii)  $\mathbb{R}_{\mathcal{S}_i} \cdot \mathbb{R}_{\mathcal{S}_j} = \mathbb{R}_{\mathcal{S}_j} \cdot \mathbb{R}_{\mathcal{S}_i}$  for  $\mathcal{S}_i \cap \mathcal{S}_j = \emptyset$ ,
- iv)  $\mathbb{R}_{\mathcal{S}_i} \cdot \mathbb{I}_{\mathcal{S}_j}$  for  $\mathcal{S}_i \subset \mathcal{S}_j$ ,
- v)  $\mathbb{I}_{\mathcal{S}_i} \cdot \mathbb{R}_{\mathcal{S}_j}$  for  $\mathcal{S}_i \cap \mathcal{S}_j = \emptyset$ .

It is noted that the operators  $\mathbb{I}_{\mathcal{S}}$  and  $\mathbb{R}_{\mathcal{S}}$  are regarded to act on the UV-finite amplitude  $\underline{M}_{\mathcal{G}}$  in which UV divergences are subtracted away by  $K$ -operations. The  $I$ -/ $R$ -subtractions are introduced in such a way that they produce IR subtraction terms as products of UV-finite quantities. To be consistent with the formal prescription for successive operations, we have adopted the definitions of Eqs. (23) and (25). However, the identification of the IR subtraction terms can be carried out diagrammatically by the form of the diagram alone, and we do not have to examine the internal UV structure of the diagram nor the explicit expressions of integrands. Thus we introduce the regulations as a formal treatment that the  $I$ -/ $R$ -operators satisfy  $\mathbb{I}_{\mathcal{S}}\mathbb{K}_{\mathcal{S}'} = 0$  and  $\mathbb{R}_{\mathcal{S}}\mathbb{K}_{\mathcal{S}'} = 0$  for  $I$ -( $R$ -)subtraction operator  $\mathbb{I}_{\mathcal{S}}$  ( $\mathbb{R}_{\mathcal{S}}$ ) for a subdiagram  $\mathcal{S}$  and a  $K$ -operation  $\mathbb{K}_{\mathcal{S}'}$  for a subdiagram  $\mathcal{S}'$ .

#### IV. CONSTRUCTION OF IR SUBTRACTION INTEGRALS

In our numerical approach, the subtraction terms are given in the form of the parametric integrals that are defined over the same Feynman parameter space as that of the original diagram. These terms are prepared so that the IR singularities of the integrand are canceled at the same point. To attain this point-by-point subtraction of the singularity associated with the IR limit, we construct the IR subtraction term  $L_{\mathcal{R}(k)}^{\mathbb{R}} \underline{M}_{\mathcal{S}}$  in such a way that the component terms  $L_{\mathcal{R}(k)}^{\mathbb{R}}$  and  $\underline{M}_{\mathcal{S}}$  expressed by separate parametric integrals are merged into a single integral by the Feynman integration formula [9, 10].

In the previous section we have seen that the IR subtraction terms can be identified by annotated forests of the diagram  $\mathcal{G}$ . By the successive applications of  $I$ -/ $R$ -subtraction operations along the forest, the form of each term is obtained as a product of component terms, which are the residual part of the vertex renormalization constants and/or that of the mass renormalization constants, and the lower-order magnetic moment part  $M$ .

In the actual construction, we follow the two-step procedure. First, we construct an integral that corresponds to a product of  $M$ ,  $\tilde{L} \equiv L - L^{\text{UV}}$  and/or  $\widetilde{\delta m} = \delta m - \delta m^{\text{UV}}$ . The location of component terms in the integration space, *i.e.* how the reduced diagrams of the components are embedded in the original diagram, is crucial to realize the point-wise subtraction. Here we introduce a tree representation of the annotated forest, called as an *annotated tree*, which provides a useful tool for identification of Feynman parameter assignment of the component integral.

In the next step we subtract away the UV subdivergences of those terms by applying  $K$ -operations that are restricted onto the respective reduced diagrams. For this purpose, we introduce an embedding tree of the annotated tree, which corresponds to a particular combination of UV subdivergences of component terms.

### A. Subtractive Integral in Feynman Parameter Space

The IR subtraction term is given as a product of component terms. Each component term is expressed as a parametric integral over the reduced diagram. Consider a case in which the IR subtraction term consists of two component terms of reduced diagrams  $\mathcal{S}$  and  $\mathcal{R} \equiv \mathcal{G}/\mathcal{S}$ . Let  $x_1, x_2, \dots, x_{n_{\mathcal{S}}}$  and  $y_1, y_2, \dots, y_{n_{\mathcal{R}}}$  be the Feynman parameters of the diagram  $\mathcal{S}$  and  $\mathcal{R}$ , and let  $x_{\mathcal{S}} = \sum_i x_i$  and  $y_{\mathcal{R}} = \sum y_i$ , respectively. Then the IR subtraction term takes the form

$$\int (dx)_{\mathcal{S}} \frac{g[\mathcal{S}]}{V_{\mathcal{S}}^{\alpha}} \times \int (dy)_{\mathcal{R}} \frac{g[\mathcal{R}]}{V_{\mathcal{R}}^{\beta}}, \quad (36)$$

where we denote the numerators of the part of integrands with the particular powers  $\alpha$  and  $\beta$  of  $V$ -function as  $g[\mathcal{S}]$  for the component of the subdiagram  $\mathcal{S}$ , and  $g[\mathcal{R}]$  for the component of the reduced diagram  $\mathcal{R}$ , respectively.

By inserting the identity

$$1 = \int_0^1 \frac{ds}{s} \delta\left(1 - \frac{x_{\mathcal{S}}}{s}\right) \int_0^1 \frac{dt}{t} \delta\left(1 - \frac{y_{\mathcal{R}}}{t}\right) \quad (37)$$

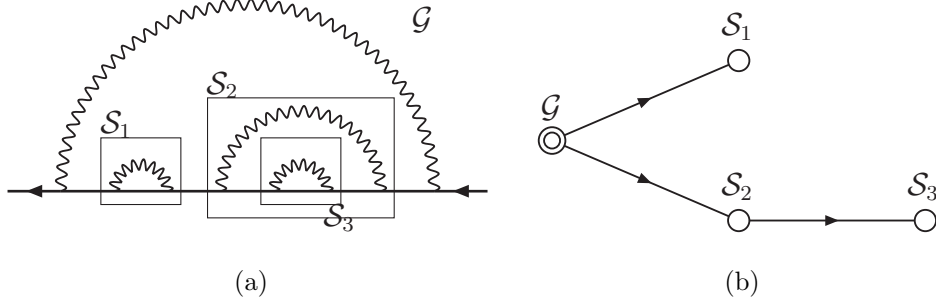
in Eq. (36) and making use of the Feynman integral formula

$$\frac{\Gamma(k)}{A^k} \frac{\Gamma(l)}{B^l} = \Gamma(k+l) \int_0^1 ds dt \delta(1-s-t) \frac{s^{k-1} t^{l-1}}{(sA + tB)^{k+l}} \quad (38)$$

the product of integrals in Eq. (36) is turned into a single integral over  $\mathcal{G}$  of the form

$$\int (dz)_{\mathcal{G}} \frac{g[\mathcal{S}] g[\mathcal{R}]}{(V_{\mathcal{S}} + V_{\mathcal{R}})^{\alpha+\beta}}, \quad (39)$$

FIG. 7: An example of nested subdiagrams of a forest and the tree representation.



where

$$\begin{aligned} z_i &= x_{\mathcal{S}} x_i & \text{for } i = 1, \dots, n_{\mathcal{S}}, \\ z_i &= y_{\mathcal{R}} y_i & \text{for } i = n_{\mathcal{S}} + 1, \dots, n_{\mathcal{G}}. \end{aligned} \quad (40)$$

By this assignment the singularities in the Feynman parameter space of both the original integrand and that of the subtraction term cancel each other. This mechanism of cancellation is crucial for our subtraction procedure.

### B. Tree Representation of Annotated Forest

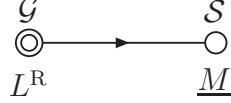
A forest is represented as a tree form that expresses the inclusion relation of the subdiagrams in the forest. (See Fig. 7.) We assign each subdiagram to a node. If a subdiagram is included in another subdiagram  $\mathcal{S}$ , it is expressed as a child node of the node assigned to  $\mathcal{S}$ . We consider the diagram  $\mathcal{G}$  itself as the root node of the tree. For later convenience, we denote the subdiagrams that contain another subdiagram  $\mathcal{S}$  as (direct) ancestors of  $\mathcal{S}$ , and the subdiagrams that are included in  $\mathcal{S}$  as descendants of  $\mathcal{S}$ .

For the annotated forest, a distinct operation of  $I$ -subtraction or  $R$ -subtraction is assigned to the node. We call such a tree as *annotated tree* hereafter. Each node is then translated into the component term of the reduced diagram.

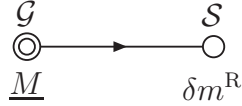
For a simplest example in which  $\mathcal{G}$  has a single subdiagram  $\mathcal{S}$ , the tree form of the forest is shown as follows:



When we consider the  $\mathbb{I}_{\mathcal{S}}$  operation, the result is given as a product of a vertex renormalization constant  $L_{\mathcal{R}(k)}^{\text{R}}$  for the part of the diagram  $\mathcal{R}(k) \equiv \mathcal{G}/\mathcal{S}(k)$  and a magnetic moment part  $\underline{M}_{\mathcal{S}}$  for the subdiagram  $\mathcal{S}$ . Those parts of subdiagrams are related to the nodes in the above tree labelled by  $\mathcal{G}$  and  $\mathcal{S}$ , respectively. Thus we represent the assignment of components of the subtraction term graphically as below.



When the  $R$ -subtraction  $\mathbb{R}_{\mathcal{S}}$  is considered, the assignment is represented in a similar manner as follows.



Here, the subdiagram  $\mathcal{S}$  referred by the right node is related to the residual self-mass term  $\delta m_{\mathcal{S}}^{\text{R}}$ , and the reduced diagram  $\mathcal{G}/\mathcal{S}(i^*)$  that corresponds to the left node is assigned to the magnetic moment part  $\underline{M}_{\mathcal{G}/\mathcal{S}(i^*)}$ .

This representation can be extended to more general cases. For an annotated forest that corresponds to a nested singularity, the successive operations of  $I$ -/ $R$ -subtractions in an appropriate order as described in Sec. III C is interpreted to extend the tree by following the respective process shown above. Then we obtain a tree representation of the annotated forest in which the nodes are assigned distinct types of  $M$ -,  $L^{\text{R}}$ -, or  $\delta m^{\text{R}}$ -nodes.

The nodes of the tree are related to the reduced diagrams, and so the annotated tree has a direct interpretation to the IR subtraction term in the form of a product of the component terms for their respective reduced diagrams. Since the tree expresses the nested structure of subdiagrams in the forest, the relevant set of Feynman parameters for the component term, *i.e.* how the reduced subdiagram for the component term is embedded in the original diagram, can be easily read off from the tree. This feature is crucial in constructing the IR subtraction integral so that the point-wise subtraction of IR singularities is achieved.

Thus far, the annotated tree provides a graphical representation of the annotated forest, and it has a one-to-one correspondence. It is readily translated into a symbolic form of the associated IR subtraction term, which is also significant for the residual renormalization step. The set of IR subtraction terms can be obtained by finding the set of annotated trees that have proper assignment of types to the nodes of tree consisted of self-energy subdiagrams.

The rules for the annotated forests given in Sec. IIIC are reflected to those for the assignment of types of components in the annotated trees. They are summarized as follows:

1. There is one and only one node to which the magnetic moment part  $\underline{M}$  is assigned.
2. The nodes that are assigned to the  $I$ -subtraction,  $L^R$ , are restricted to the ancestor nodes of the magnetic moment part.
3. The nodes that are assigned to the residual self-mass subtraction,  $\delta m^R$ , do not appear as the ancestor nodes of the magnetic moment part.

It turns out that to fulfill these rules the assignment is uniquely determined once a node is chosen for the magnetic moment part. We first pick up a node that is assigned to the magnetic part  $\underline{M}$ , and then the nodes that lie as ancestors of the  $M$ -node are associated with the  $I$ -subtractions. The remaining nodes are assigned to the  $R$ -subtractions.

### C. Subtraction of UV Subdivergences

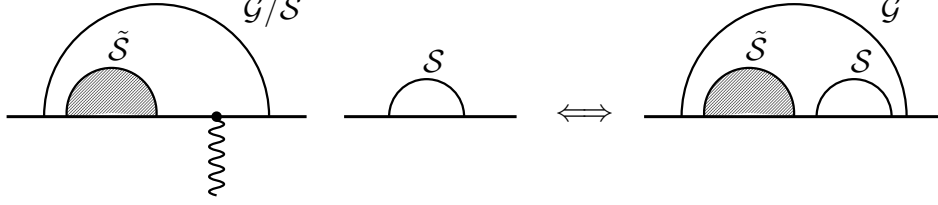
We now proceed to the treatment of UV subdivergences in the components of IR subtraction terms. For example, the residual part of vertex renormalization constant  $L^R$  is given in the form

$$L_{\mathcal{R}(k)}^R = L_{\mathcal{R}(k)} - L_{\mathcal{R}(k)}^{\text{UV}} + \sum_{f \in \mathfrak{F}} \prod_{S' \in f} (-\mathbb{K}_{S'}) \tilde{L}_{\mathcal{R}(k)}. \quad (41)$$

We have introduced a term  $\tilde{L}_{\mathcal{R}(k)} \equiv L_{\mathcal{R}(k)} - L_{\mathcal{R}(k)}^{\text{UV}}$  in the construction of the subtraction term which is given from  $L_{\mathcal{R}(k)}$  by dropping the most-contracted term  $L_{\mathcal{R}(k)}^{\text{UV}}$ . The divergences that originate from the substructure have to be subtracted away that are dealt with  $K$ -operations for the forests  $f$  of  $\mathcal{R}(k)$ . In this section we show that these subdivergences can be handled in a systematic way and present it as a general scheme.

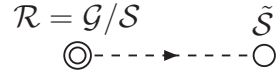
The IR subtraction term constructed in the previous section is originally given as a product of separate integrals defined on the respective component diagrams. As an example, the term  $L_{\mathcal{R}(k)}^R \underline{M}_{\mathcal{S}}$  is made of the vertex renormalization constant defined for the vertex diagram  $\mathcal{R}(k)$  and the magnetic moment part defined for the diagram  $\mathcal{S}$ . Those components have their own divergent subdiagrams.

FIG. 8: A UV divergent subdiagram  $\tilde{\mathcal{S}}$  in the annotated forest  $\{\mathcal{G}, \mathcal{S}\}$ .



It is shown that these subdiagrams of separate components can be mapped to subdiagrams of the original diagram  $\mathcal{G}$ . A subdiagram  $\tilde{\mathcal{S}}$  of a component diagram is itself a subdiagram of  $\mathcal{G}$ , or  $\tilde{\mathcal{S}}$  is obtained as a reduced diagram by shrinking other component diagrams.

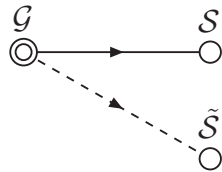
Thus, it can be recognized graphically in a way that a forest of a component diagram is related to a forest of the original diagram. The tree form of the forest of the component diagram can be embedded as a subtree of the original annotated forest that corresponds to the IR subtraction term by mapping the elements of the subtree as that of the original forest. We call such a tree that corresponds to UV subdivergence of certain components the embedding tree. For example, consider a case in which the component diagram  $\mathcal{R} = \mathcal{G}/\mathcal{S}$  has a forest consisting of a subdiagram  $\tilde{\mathcal{S}}$  as shown in Fig. 8. The tree form of this forest



is embedded in the annotated forest



which reduces to the forest of the whole diagram  $\mathcal{G}$  shown as follows.



It is noted that the component diagrams are disjoint by construction and therefore the subdiagrams of different component diagrams are not overlapping.

The UV subdivergences contained in the product of the components are identified by forests of the original diagram  $\mathcal{G}$ . For the annotated forest  $\tilde{f}$  that corresponds to the IR subtraction term, consider a forest  $f'$  that includes  $\tilde{f}$ , in the sense that all subdiagrams of

$\tilde{f}$  are also the elements of  $f'$ . Then the subdiagrams in  $f' - \tilde{f}$ , *i.e.* the subdiagrams of  $f'$  that are not in  $\tilde{f}$ , are related to the subdivergences of the component diagram to which they belong respectively. The subtraction term of the UV subdivergence is constructed by applying  $K$ -operations for these subdiagrams restricted onto the corresponding component diagram. For example,  $\mathbb{K}_{\tilde{\mathcal{S}}}$  acts on the component  $\mathcal{G}/\mathcal{S}$  in Fig. (8).

Therefore, the UV subdivergences for an IR subtraction term that originate from the distinct component terms are synthetically identified by the forests of the original diagram  $\mathcal{G}$ . However, not all the subdiagrams of  $\mathcal{G}$  cause divergences of the IR subtraction term related to the annotated forest  $\tilde{f}$ . Consider a case in which a vertex subdiagram  $\mathcal{S}'$  includes a self-energy subdiagram  $\mathcal{S}$ , *i.e.*  $\mathcal{S}' \supset \mathcal{S}$ . For the  $I$ -subtraction associated with  $\mathcal{S}$ , the subdiagram  $\mathcal{S}$  is replaced by an external vertex. Thus  $\mathcal{S}'$  acquires the extra vertex in the reduced diagram  $\mathcal{G}/\mathcal{S}(k)$  and becomes irrelevant for the UV divergence. We have to exclude such cases from the identification of subdivergences.

Another rule must be imposed in relation to the residual self-mass subtraction. First consider a nested UV divergences in which self-energy subdiagram  $\mathcal{S}$  is included in a vertex or another self-energy subdiagram  $\tilde{\mathcal{S}}$ . There would be a UV subtraction term denoted as  $\delta m_{\mathcal{S}}^{\text{UV}} L_{\tilde{\mathcal{S}}/\mathcal{S}(i^*)}^{\text{UV}}$  for the vertex subdiagram, or  $\delta m_{\mathcal{S}}^{\text{UV}} B_{\tilde{\mathcal{S}}/\mathcal{S}(i^*)}^{\text{UV}}$  for the self-energy subdiagram in the prescription of  $K$ -operation. However, by construction of  $K$ -operation it is found that those terms that involve the most-contracted part of the vertex renormalization constants or wave-function renormalization constants with mass insertions do not actually appear. Accordingly, we also have to omit the residual self-mass term  $\delta m_{\mathcal{S}}^{\text{R}} L_{\tilde{\mathcal{S}}/\mathcal{S}(i^*)}^{\text{UV}}$  or  $\delta m_{\mathcal{S}}^{\text{R}} B_{\tilde{\mathcal{S}}/\mathcal{S}(i^*)}^{\text{UV}}$ , respectively. They would be realized as UV subdivergences of the component  $\tilde{\mathcal{S}}/\mathcal{S}$ .

## V. PROCEDURE AND IMPLEMENTATION

In this section we describe the flow of process to generate the numerical integration code for IR subtraction terms of a  $q$ -type diagram from its representation.

We first identify the IR divergent parts based on the forest structure of the diagram and provide the set of subtraction terms as annotated forests. Next we identify the UV subdivergences of these IR subtraction terms. The subtraction terms for these subdivergences are constructed by applying  $K$ -operations to the IR subtraction integrals.

The subtraction terms of IR divergences and their UV subdivergences thus constructed

are turned into FORTRAN codes. They are merged to the numerical calculation codes for UV finite amplitude generated by the scheme developed in Ref. [10]. The entire flow of process is depicted in Fig. 9. The numerical integration codes are readily integrated by VEGAS to produce a finite amplitude for the diagram. Some of the steps are common to the procedure for UV subtraction described in Ref. [10].

### A. Finding Forest Structures

The types of subdiagrams that are relevant to the IR subtraction term and their UV subdivergences are self-energy subdiagrams and vertex subdiagrams. For a *q-type* diagram a subdiagram of these types is represented by a segment of the lepton path. All subdiagrams of a diagram are thus found by examining all segments that correspond to the connected one-particle irreducible subdiagrams of vertex type or self-energy type.

The inclusion relation of the subdiagrams are thus mapped to that of the segments. Once it is found, the whole set of (normal) forests is found by generating all possible combinations of subdiagrams and disregarding any combinations in which a pair of elements are overlapping.

For each forest we examine the nest structure of subdiagrams and describe it in a tree form whose root node is associated with the whole diagram  $\mathcal{G}$ .

### B. Finding IR Subtraction Term

The IR divergences of a *q-type* diagram emerge in relation to subdiagrams of the self-energy type. To identify the divergence structure, we first pick out the forests that consist of only self-energy subdiagrams. Suppose they are expressed in a tree form. Next, we assign to each node of the tree the type of component of subtraction term among the choices: the residual part of vertex renormalization constant ( $L^R$ ) that is related to *I*-subtraction, the residual self-mass part ( $\delta m^R$ ) that is related to *R*-subtraction, and the magnetic moment part ( $\underline{M}$ ). The assignment that fulfills the rules in Sec. III can be found by following steps.

1. Choose a node for the magnetic moment part (denoted by *M*-node).
2. The ancestor nodes of *M*-node are assigned to the  $L^R$ -part (denoted by  $L^R$ -node).



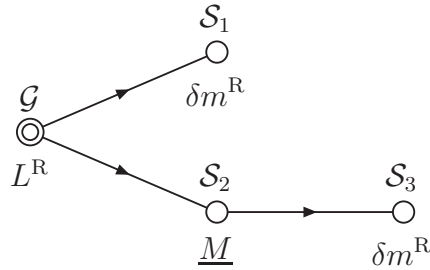
3. Other nodes are assigned to the residual self-mass parts (denoted by  $\delta m^{\text{R}}$ -node).

We call the forest with proper assignment of types to the nodes of its tree representation as the annotated forest. Each annotated forest corresponds to a IR subtraction term.

The expression of the IR subtraction term associated with the annotated forest is then given in a form of a product of component terms that are related to the nodes of the tree. The component term of a node  $\mathcal{S}$  is found by following the rules below.

- An  $L^{\text{R}}$ -node corresponds to the residual part of the vertex renormalization constant  $L_{\mathcal{R}(k)}^{\text{R}}$  for the diagram  $\mathcal{R}(k)$ . It is obtained from  $\mathcal{S}$  by replacing the inner subdiagram that is assigned to  $M$ -node or  $L^{\text{R}}$ -node by a vertex  $k$ , and by shrinking the subdiagrams of child nodes to points.
- A  $\delta m^{\text{R}}$ -node corresponds to the residual part of the mass renormalization constant  $\delta m_{\mathcal{R}}^{\text{R}}$  for the diagram  $\mathcal{R}$ . It is obtained from  $\mathcal{S}$  by shrinking the subdiagrams of child nodes to points.
- An  $M$ -node corresponds to the magnetic moment part  $\underline{M}_{\mathcal{R}}$  for the diagram  $\mathcal{R}$  obtained from  $\mathcal{S}$  by shrinking the subdiagrams of child nodes to points.

As an example, consider an annotated tree shown as



It corresponds to the IR subtraction term

$$L_{\mathcal{G}/\mathcal{S}_1/\mathcal{S}_2(k_2)(i_1^*)}^{\text{R}} \delta m_{\mathcal{S}_1}^{\text{R}} \underline{M}_{\mathcal{S}_2/\mathcal{S}_3(i_3^*)} \delta m_{\mathcal{S}_3}^{\text{R}}. \quad (42)$$

Since the mass renormalization constant of second order  $\delta m_2$  satisfies  $\delta m_2^{\text{UV}} = \delta m_2$ , the residual self-mass subtraction for the second-order self-energy subdiagram is not necessary. We omit the annotated forests that involve such cases.

An example of a complete set of IR subtraction terms for an eighth-order diagram identified in the above procedure is shown in Appendix A.

### C. Constructing IR Subtraction Integral

The integrand of the IR subtraction term associated with an annotated forest  $\tilde{f}$  is constructed by the following steps. First we identify the position of each component term in the original diagram  $\mathcal{G}$ , and find the respective sets of Feynman parameters for those components. This step is crucial for our numerical method based on the point-by-point subtraction. Then we follow these steps:

1. Construct the integrand as a product of those of component terms.
2. Find the building blocks,  $B_{ij}$ ,  $U$ ,  $C_{ij}$  and  $A_i$ .
3. Construct the  $V$ -function in a form that guarantees the analytical factorization of the subtraction integral into components.

#### 1. Integrand

The numerator of the integrand of the subtraction term is given as a product of those of component terms. We first consider the full part of the component integrands, the vertex renormalization constant  $L$ , the mass renormalization constant  $\delta m$ , and the magnetic part  $M$ , before dropping other than the residual part.

For example, consider an annotated forest consisted of an  $I$ -subtraction for the subdiagram  $\mathcal{S}$ . We construct the subtraction term of the form of product

$$\tilde{L}_{\mathcal{R}(k)} M_{\mathcal{S}}. \quad (43)$$

The numerator of the integrand (except for the numerical constants) is thus given by

$$\text{Tr}_{\mathcal{R}(k)} \left\{ P_{\nu} \gamma^{\alpha} (\not{p} - m) \cdots \not{p}_k^{\nu} \cdot \text{Tr}_{\mathcal{S}} \left\{ P \gamma^{\beta} (\not{p} - m) \cdots \gamma_{\beta} \right\} \cdot (\not{p} - m) \cdots \gamma_{\alpha'} \right\}, \quad (44)$$

where the labels  $\mathcal{R}(k)$  and  $\mathcal{S}$  of the traces indicate that the traces are taken separately for the components in  $\mathcal{R}(k)$  and  $\mathcal{S}$ .  $P_{\nu}$  and  $P$  are the projection operators for the vertex renormalization constant and the magnetic moment, respectively, and the term  $\not{p}_k$  refers to the external vertex  $k$ .

The expression (44) is analogous to the integrand of the unrenormalized amplitude of the original diagram  $\mathcal{G}$  except for these points:

- There are multiple traces, each of which corresponds to the respective component term.
- Each part has appropriate projection operator inserted.
- For the  $L^R$ -parts associated with the  $I$ -subtractions, extra vertices are inserted.

On the other hand, the pattern of contractions of the internal vertices by the photon propagators is the same as that of the original diagram  $\mathcal{G}$  given by the pairings of the diagram representation. Thus we construct the integrand of the subtraction term based on that of the unrenormalized amplitude by incorporating modifications listed above.

We perform the trace operations, and turn the integrand into a Feynman parametric form by carrying out the momentum integration analytically using the integration table. The result is expressed as a polynomial of the symbols called the building blocks,  $B_{ij}$ ,  $U$ ,  $C_{ij}$ ,  $A_i$  and  $V$ , each of which is given as a function of Feynman parameters.

We have to remove the leading overall UV divergent parts of the component terms  $L$  and  $\delta m$  to leave their residual parts. It is achieved by dropping the most-contracted term of the component integral which can be identified by simple power counting.

## 2. Building Blocks

The integrand of the IR subtraction term is constructed as a product of component terms, each of which is defined on the distinct set of Feynman parameters and given in the form of rational function of building blocks that are also defined on the respective component diagram. However, we need not prepare these building blocks separately if we recall that the building blocks  $B_{ij}$  and  $U$  factorize exactly in the UV limit.

In the UV limit associated with a subdiagram  $\mathcal{S}$ , the building blocks  $B_{ij}$  and  $U$  factorize in the form

$$U_{\mathcal{G}} \rightarrow U_{\mathcal{G}/\mathcal{S}} \cdot U_{\mathcal{S}}, \quad (45)$$

$$\left. \frac{B_{ij}}{U} \right|_{\mathcal{G}} \rightarrow \left. \frac{B_{ij}}{U} \right|_{\mathcal{S}} \quad \text{for } i, j \in \mathcal{S}, \quad (46)$$

$$\left. \frac{B_{ij}}{U} \right|_{\mathcal{G}} \rightarrow \left. \frac{B_{ij}}{U} \right|_{\mathcal{G}/\mathcal{S}} \quad \text{for } i, j \in \mathcal{G}/\mathcal{S}, \quad (47)$$

where the labels  $\mathcal{G}$ ,  $\mathcal{S}$ , and  $\mathcal{G}/\mathcal{S}$  denote that the quantities are defined on the respective diagrams.

Therefore, we are able to use the building blocks  $B_{ij}$  and  $U$  obtained in the UV limit associated with the same forest  $f$ . We have to eliminate unwanted contributions by explicitly putting the elements of  $B_{ij}$  to zero for  $i \in \mathcal{S}$  and  $j \notin \mathcal{S}$  to ensure that the integrand originates from the separate integrals.

### 3. *V-function*

In order that the exact factorization of the integrand holds, the  $V$ -function in the denominator of the integrand is constructed in the form

$$V \rightarrow \sum_{\mathcal{S}} V_{\mathcal{S}}, \quad (48)$$

where the sum is taken over the component diagrams.

## D. Subtraction Terms for UV Subdivergences

The integral forms of the subtraction terms for UV subdivergences that originate from the components of the IR subtraction term are constructed by the following steps. We assume that the IR subtraction term is associated with the annotated forest  $\tilde{f}$ .

### 1. *Identification of Subdivergences*

The set of UV subdivergences to the annotated forest  $\tilde{f}$  is given by finding forests  $f'$  that include  $\tilde{f}$ . The emergence of UV subdivergences are associated with the subdiagrams in  $(f' - \tilde{f})$ , *i.e.* the subdiagrams of  $f'$  that are not the elements of  $\tilde{f}$ . By the tree forms of the forests  $f'$  and  $\tilde{f}$  we identify which component of IR subtraction term each of these subdiagrams belongs to. We check if these subdiagrams in the component diagrams actually cause the divergences, and disregard the cases described in Sec. IV C.

## 2. *Integrand*

The integrand of the subtraction term for the UV subdivergence is obtained by applying the set of  $K$ -operations identified in the previous step. The individual  $K$ -operation is carried out by the power counting in a similar manner as the ordinal  $K$ -operations except that the domain of operation is restricted to the corresponding component diagram that the subdiagram belongs to. When there are more than one subdiagram, the  $K$ -operations are applied successively. The order of applications to different components is indifferent to the result. For a proper definition of the integrand Feynman cutoff must be introduced for UV-divergent subdiagrams. Of course, the cutoff dependence cancels out in the end.

## 3. *Building Blocks*

For each component diagram, the building blocks for the subtraction term of the UV subdivergence are obtained in the factorized form for the respective UV limit. Recall that the building blocks of the IR subtraction term for the annotated forest  $\tilde{f}$  is given as those obtained for the UV subtraction term associated with the same forest. Thus they reduce to the building blocks  $B_{ij}$  and  $U$  in the UV limit of the forest  $f'$ .

## E. **Implementation**

We implemented the steps described above as separate Perl programs that use internally FORM [15] and Maple. These symbolic manipulation programs take traces, project out the magnetic moment, perform analytic integration over momentum variables by means of home-made integration tables written in FORM, carry out inversion of matrices which creates  $B_{ij}$  and  $U$ , and execute  $K$ -operations. The programs for the IR subtraction part are integrated with the programs that generate the codes for UV-finite amplitudes previously developed [10], to form the automated code-generating system for the finite amplitude free from both UV and IR divergences.

The code-generating system takes the name of the diagram and finds the corresponding single-line expression of the diagram from the table prepared beforehand. Then it generates the numerical integration code in FORTRAN format that consists of the unrenormalized amplitude and appropriate subtraction terms. The FORTRAN code is readily integrated

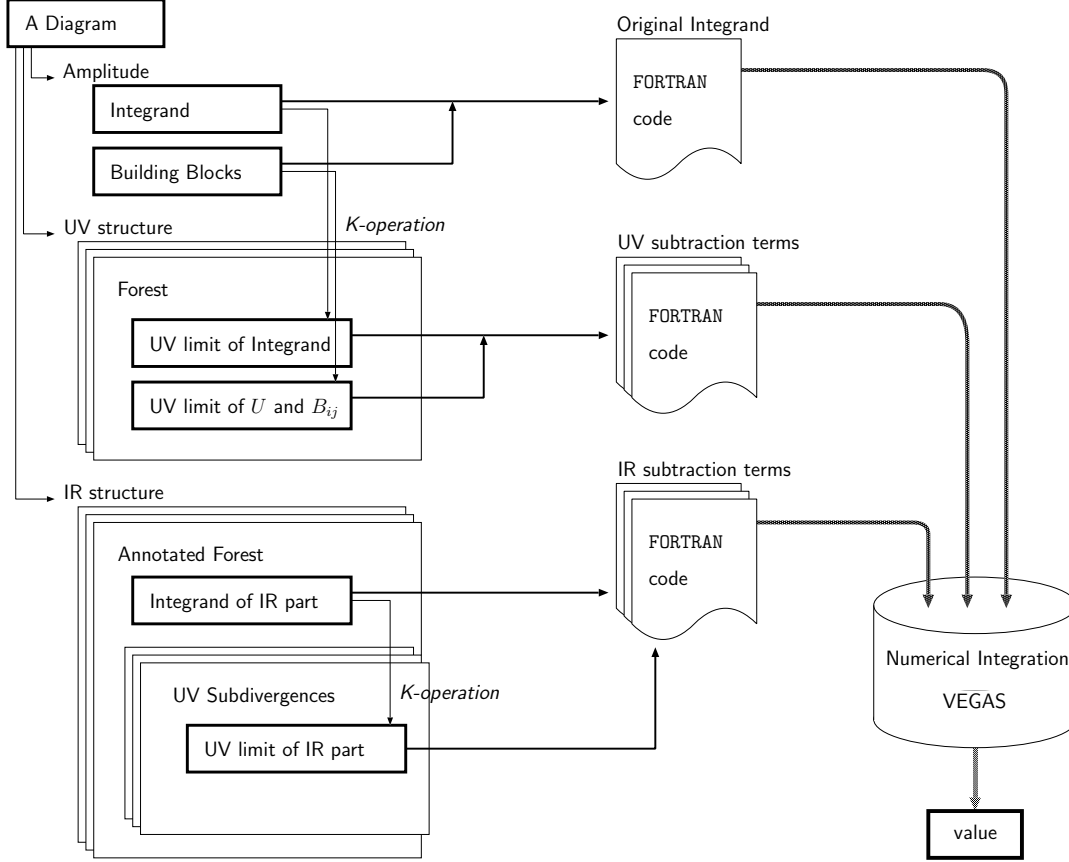


FIG. 9: Flow of automated code generation.

by a numerical integration program, to which purpose we use VEGAS [11], an adaptive Monte-Carlo integration routine.

The whole steps are controlled by `make` utility and a shell script. It is noted that some steps are independent with each other so that they can be performed simultaneously. By specifying appropriate options to `make`, those operations are performed in parallel. This feature is beneficial in the present multi-processor/multi-core computer environment.

## VI. CONCLUSION AND DISCUSSION

In this article we described a systematic procedure for the construction of IR subtraction terms in the calculation of lepton anomalous magnetic moment. Our present concern is the type of diagrams without internal lepton loops (called *q-type* diagrams) that account for a significant fraction and the most difficult portion of calculation of QED corrections to lepton  $g-2$ . We presented a procedure for the automated generation of the numerical

integration code, which, together with the previously developed automation scheme for UV-finite amplitude, provides prescription for the fully-renormalized and finite amplitude.

We implemented the code-generating system based on our procedure as a set of Perl programs that work with the helps of symbolic manipulation systems, FORM and Maple. The entire flow of process is managed by `make` utility and a shell script. It generates numerical integration code in FORTRAN format, which is readily integrated by numerical integration system, VEGAS. Our implementation is applicable to any order of diagrams of *q-type*.

For the purpose of debugging of our automation system we have applied it to the evaluation of known diagrams of sixth- and eighth-orders. The sixth-order contribution of *q-type* diagrams comes from fifty vertex diagrams, which are reduced to eight self-energy-like diagrams taking account of the Ward-Takahashi identity and the time-reversal symmetry. It takes just one minute to create all eight FORTRAN programs for  $M_{6\alpha}$  ( $\alpha = a, b, \dots, h$ ) on *hp*'s Alpha machine. Numerical evaluation was carried out on RIKEN's cluster system (RSCC). The result obtained is, after incorporating the residual renormalization,

$$A_1^{(6)}(\text{q-type}) = 0.9052 \quad (49)$$

which reproduces the exact result [16] quite satisfactorily

$$A_1^{(6)}(\text{q-type})_{\text{exact}} = 0.904979 \dots \quad (50)$$

The value (49) was obtained by computation by VEGAS of 2 – 6 hours wall-clock time with 16 Xeon-CPU's for each diagram, which sampled one hundred million points per iteration and 450 iterations.

The eighth-order *q-type* diagrams consist of 518 vertex diagrams, which are reduced to 47 self-energy-like diagrams with the help of the Ward-Takahashi identity and the time-reversal symmetry. The entire 47 program sets are generated by our automated code-generating system in less than ten minutes on *hp*'s Alpha machine. The numerical evaluation is, however, quite non-trivial and requires huge computational resources. For the preliminary evaluation we have used 64 to 256 CPU's per diagram for a few months on RSCC to reach the relative uncertainty of about 3 %.

One unexpected byproduct is that it revealed an inconsistency in the treatment of IR subtraction terms in the previous calculation of the eighth-order *q-type* diagrams [17]. With

this inconsistency resolved, the new and old calculations agreed within the numerical precision employed. Note that this is the first time that the complete eighth-order contribution to  $g-2$  has been calculated by more than one independent method. The agreement of two independent calculations puts the eighth-order contribution to  $a_e$  on a firm ground, and advances the test of QED and the determination of the fine structure constant derived from  $a_e$  to a higher level of precision.

These tests have confirmed the validity of our automation system, and encouraged us to tackle the evaluation of the tenth-order contribution with confidence. Of 6354 *q-type* vertex diagrams that contribute to the tenth-order term, 2232 diagrams that have only vertex subdiagrams have already been evaluated [10]. For the remaining 4122 diagrams that have self-energy subdiagrams and thus suffer from the infrared singularity, we are evaluating their Ward-Takahashi version (254 diagrams) by the automation system described in this article. It seems thus far that the numerical results of these diagrams are finite and our subtraction scheme works as expected. Some diagrams show somewhat unstable behavior during the evaluation which seems to indicate the presence of a severe digit-deficiency problem<sup>4</sup>. To deal with such cases we have modified the code so that we can carry out the integration with extended numerical precision.

It is important to note that our new subtraction scheme for IR divergences differs from the scheme described in Ref. [9] by finite quantity. In the previous approach, the IR subtraction term was chosen for a self-energy subdiagram  $\mathcal{S}$  in the form of Eq. (13) defined by the  $I$ -operation alone. In the new scheme, we have chosen the form  $L_{\mathcal{R}(k)}^R$  for the subtraction term defined as the residual part of  $L_{\mathcal{R}(k)}$  other than the UV divergences. This choice of term includes a finite part  $\Delta L$  in the previous calculations. Thus the subtraction of the nested IR singularity is carried out differently. The latter part of Eq. (13) is related to our residual self-mass subtraction, but the form of term  $M_{\mathcal{R}^*}[I]$  was chosen through the careful inspection of the divergent structure of the particular diagram.

Therefore the previous scheme and the new scheme yield different integrals for diagrams containing self-energy subdiagrams. The difference can be traced analytically. In the eighth-order case it is confirmed by numerical calculation. The difference is, of course, to be compensated by the different set of terms for the residual renormalization step.

---

<sup>4</sup> For a detailed discussion of digit-deficiency problem, see Appendix B of Ref. [18].



In this series of articles we have focused on the particular type of diagrams that have no lepton loops (*q-type*). However, our procedure is readily applicable to other types of diagrams that are obtained by inserting vacuum polarizations to *q-type* diagrams. Such sets of diagrams of the tenth order are [8, 10]

- Set III(a) obtained from the sixth-order *q-type* diagrams by inserting two second-order vacuum polarizations,
- Set III(b) obtained from the sixth-order *q-type* diagrams by inserting a fourth-order vacuum polarization,
- Set IV obtained from the eighth-order *q-type* diagrams by inserting a second-order vacuum polarization.

The automated code generation for these sets is accomplished with only small modifications to the code. The integration codes have already been obtained, and the numerical evaluation has been carried out. The result will be reported elsewhere.

### Acknowledgments

This work is supported in part by JSPS Grant-in-Aid for Scientific Research (C)19540322. T. K.'s work is supported by the U. S. National Science Foundation under Grant PHY-0355005. M. H.'s work is supported in part by JSPS and the French Ministry of Foreign Affairs under the Japan-France Integrated Action Program (SAKURA). The numerical calculation has been performed on the RIKEN Super Combined Cluster System (RSCC).

### APPENDIX A: IDENTIFICATION OF IR SUBTRACTION TERMS: AN EXAMPLE

As a demonstration of the IR subtraction scheme, we present the identification of IR subtraction terms for an eighth-order diagram,  $M_{18}$ , shown in Fig. 10.

The diagram  $M_{18}$  has three self-energy subdiagrams denoted by  $\mathcal{S}_1$ ,  $\mathcal{S}_2$ , and  $\mathcal{S}_3$ . The number of combinations of those subdiagrams (forests) is seven, and the number of ways to assign the types ( $M$ ,  $L^R$ , or  $\delta m^R$ ) to the nodes is 19. Dropping the cases that contain the second-order residual self-mass subtractions  $\delta m_2^R = 0$ , it is found that the IR subtraction

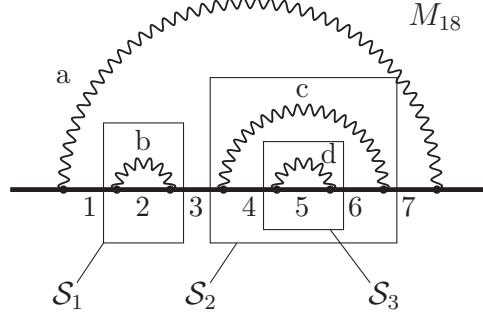
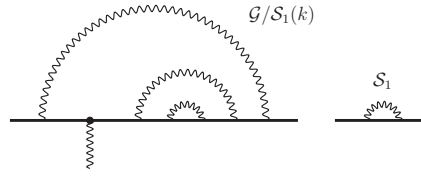


FIG. 10: An eighth-order diagram  $M_{18}$ . The numerals denote the indices of lepton lines and the roman alphabets denote the indices of photon lines. The diagram  $M_{18}$  has three self-energy subdiagrams denoted by  $S_1$ ,  $S_2$ , and  $S_3$ .

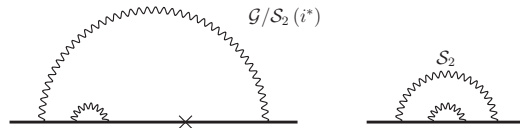
terms are given by the following six cases. On the left-hand side is shown the annotated tree, and the figure on the right-hand side expresses the reduced subdiagrams of the component terms.

As a convention we denote the subtraction term by the symbol  $I$  and/or  $R$  with suffixes that refer to the indices of lepton lines. They are the indices to lepton lines contained in  $L^R$  for  $I$ -subtraction, and the range of indices to lepton lines indicated by the left-most and the right-most indices contained in  $\delta m^R$  for  $R$ -subtraction.

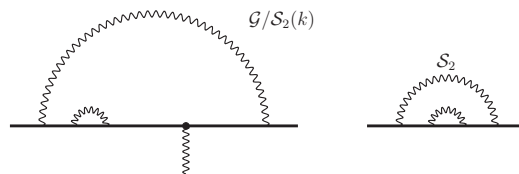
- $I_{134567}$



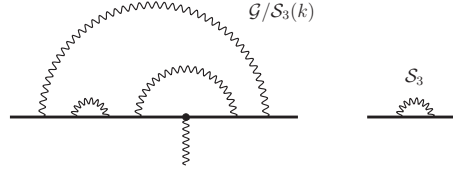
- $R_{46}$



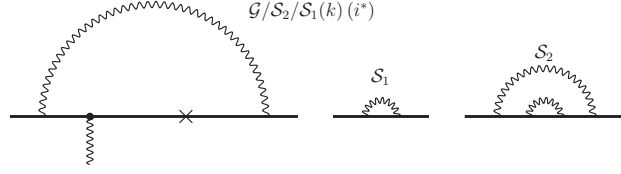
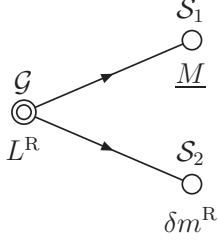
- $I_{1237}$



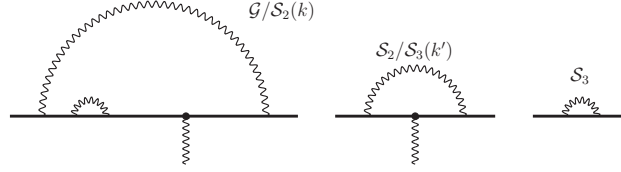
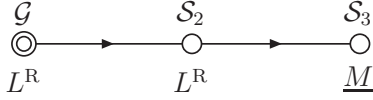
- $I_{123467}$



- $I_{137}R_{46}$



- $I_{1237}I_{46}$



- 
- [1] P. Kusch and H. M. Foley, Phys. Rev. **72**, 1256 (1947).
- [2] R. S. Van Dyck, P. B. Schwinberg, and H. G. Dehmelt, Phys. Rev. Lett. **59**, 26 (1987).
- [3] B. Odom, D. Hanneke, B. D'Urso, and G. Gabrielse, Phys. Rev. Lett. **97**, 030801 (2006).
- [4] G. Gabrielse, D. Hanneke, T. Kinoshita, M. Nio, and B. Odom, Phys. Rev. Lett. **98**, 039902(E) (2007).
- [5] P. J. Mohr and B. N. Taylor, Rev. Mod. Phys. **77**, 1 (2005).
- [6] K. Melnikov and A. Vainshtein, Phys. Rev. **D70**, 113006 (2004).
- [7] G. Gabrielse, D. Hanneke, T. Kinoshita, M. Nio, and B. Odom, Phys. Rev. Lett. **97**, 030802 (2006).
- [8] T. Kinoshita and M. Nio, Phys. Rev. D **73**, 053007 (2006).
- [9] T. Kinoshita, in *Quantum electrodynamics*, edited by T. Kinoshita (World Scientific, Singapore, 1990), pp. 218–321, (Advanced series on directions in high energy physics, 7).
- [10] T. Aoyama, M. Hayakawa, T. Kinoshita, and M. Nio, Nucl. Phys. B **740**, 138 (2006).
- [11] G. P. Lepage, J. Comput. Phys. **27**, 192 (1978).

- [12] T. Kinoshita and W. B. Lindquist, Phys. Rev. D **42**, 636 (1990).
- [13] P. Cvitanović and T. Kinoshita, Phys. Rev. D **10**, 3978 (1974).
- [14] P. Cvitanović and T. Kinoshita, Phys. Rev. D **10**, 3991 (1974).
- [15] J. A. M. Vermaseren (2000), math-ph/0010025.
- [16] S. Laporta and E. Remiddi, Phys. Lett. **B379**, 283 (1996).
- [17] T. Aoyama, M. Hayakawa, T. Kinoshita, and M. Nio (2007), arXiv:0706.3496 [hep-ph].
- [18] T. Kinoshita and M. Nio, Phys. Rev. **D70**, 113001 (2004).